REVIEW

*This section of Journal of Materials Research is reserved for papers that are reviews of literature in a given area.*

# Conceptual progress for explaining and predicting semiconductor properties

Marvin L. Cohen[a)]
*Department of Physics, University of California at Berkeley, Berkeley, California 94611; and Materials Sciences Division, Lawrence Berkeley National Laboratory, Berkeley, California 94720*

(Received 4 June 2011; accepted 1 September 2011)

After some background discussion, this review will focus on some recent developments in the areas of theoretical studies of semiconductor electronic structure, photovoltaics, semiconducting boron nitride nanotubes, and the search for modified semiconductors and insulators with higher superconducting transition temperatures. The background discussion covers the evolution of studies of solids, which changed dramatically after the development of quantum theory. These conceptual changes resulted in methods for calculating properties of materials and theoretical frameworks for interpreting experimental measurements. In some cases, the theoretical approaches have been successful in predicting new materials and new properties. As stated above, a few examples will be given to illustrate the development of this field.

## I. INTRODUCTION

The prehistory of theoretical work on condensed matter systems involves the belief that solids are made of atoms and atoms can be understood using quantum theory. The first part goes back to theorists like Einstein, Boltzmann, and Drude at the beginning of the last century, whereas the second part relies on the atomic and quantum theories of Bohr, Dirac, Schrödinger, Heisenberg, and others in the 1920s. Calculating properties of solids based on knowing about the properties of their constituent atoms started in the 1920s and 1930s with the work of Born, Sommerfeld, Bethe, and others, but the actual applications to explaining and predicting properties of solids took many years. As in the study of atoms, a critical part in developing an atomic and ultimately a quantum theory was the use of optical spectral studies. However, because solid state spectra are broad and relatively featureless compared to atomic spectra, unraveling their message was difficult.

In the 1960s and 1970s, the optical properties of semiconductors originating from interband electronic transitions were essentially explained by an international experimental–theoretical collaboration.[1] On the experimental side, reflectivity, modulated reflectivity, and photoemission techniques provided the theorists with reliable data to build semiempirical theories. The most popular of these was the empirical pseudopotential method (EPM),[2,3] where the crystalline potential was determined by comparing the calculated optical properties with the experimental data. This approach was not just a fitting scheme. It was based on a theoretical model in which each ion of the crystal had an appropriate potential to simulate valence electron–ion interactions. In addition, the application of the method focused on fundamental problems connected with exploring electronic behavior in crystals. Eventually, this set the stage for the development of ab initio theories and methods that are in use today.

These modern ab initio theories can be applied to a wide variety of properties for a large class of solids, clusters, molecules, and nanostructures. The latest methods describe ground and excited state properties such as: electronic structure, crystal structures and structural transitions, structural and mechanical properties, lattice vibrational properties, electron–lattice interactions, superconductivity, optical properties, photoemission spectra, etc.

Not only have these approaches helped in explaining properties but also they have been predictive. After some details about the methodology, we will focus on a few examples where the methods have been applied with success.

## II. PSEUDOPOTENTIALS

In the 1930s, Fermi,[4] Hellmann,[5] and others explored the construction of a pseudopotential to give the electron–ion interaction. Over the years, many forms have been introduced and used with success. If one adopts a model of a crystal as a periodic array of pseudoatoms or cores surrounded by a gas of valence electrons as shown in Fig. 1, then in the case of the EPM, all that is needed is an average potential to reproduce the optical data. In the 1950s, Phillips and Kleinman[6] showed that because the Pauli principle forced valence electrons to stay out of the regions where the core electrons are, this could be represented by a repulsive potential in this region that

[a)]Address all correspondence to this author.
e-mail: mlcohen@berkeley.edu
DOI: 10.1557/jmr.2011.328

 © Materials Research Society 2011 

https://doi.org/10.1557/jmr.2011.328 Published online by Cambridge University Press

would cancel part of the attractive potential of the ionic core and produce a weak pseudopotential. A typical pseudopotential $V(r)$ for an ion is shown in Fig. 2. Assuming Fermi–Thomas screening by free electrons, the Fourier transform of $V(r)$, $V(q)$ is shown in Fig. 3. For electronic band structure calculations, we only need the values of $V(q = \boldsymbol{G})$, where $\boldsymbol{G}$ is a reciprocal lattice vector. This is shown in Fig. 3.

For systems like diamond, Si, and Ge in the diamond structure, only the first three $\boldsymbol{G}$ values for $V(\boldsymbol{G})$ need to be considered. Hence by fitting just three Fourier coefficients or form factors, it is possible to get a band structure $E(k)$ which is in agreement with the experimental data to within a few tenths of an electron volt over a range of a Rydberg.

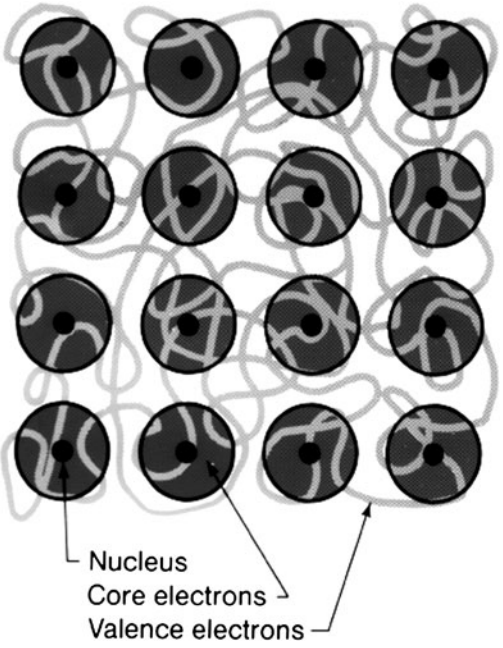



FIG. 1. Pseudopotential model with cores in a sea of valence electrons.

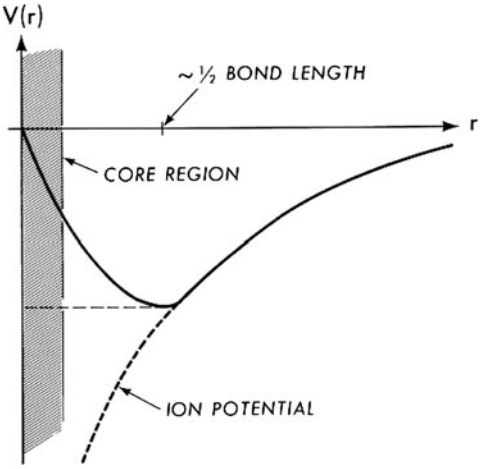



FIG. 2. Schematic drawing of a real space pseudopotential.

Not only were the energy levels accurate, the electronic density obtained by squaring the pseudo wave function gave a successful prediction of the x-ray results measuring the valence electron density.[1] So the EPM approach shown in Fig. 4 was highly successful in interpreting many properties of semiconductors and explained the optical properties as explained earlier.

The next advance was to create the potentials from first principles using only the atomic number as input. This was achieved in several ways. The usual approach was to construct a potential which gave the same results as that obtained for an all-electron atomic calculation, but with a smooth nodeless tail in the core region[7–9] as shown in Fig. 5. With this potential to express the electron–core interaction, the Coulomb core–core interaction, the Hartree mean field electron–electron interaction, and the electronic exchange–correlation contribution calculated using density

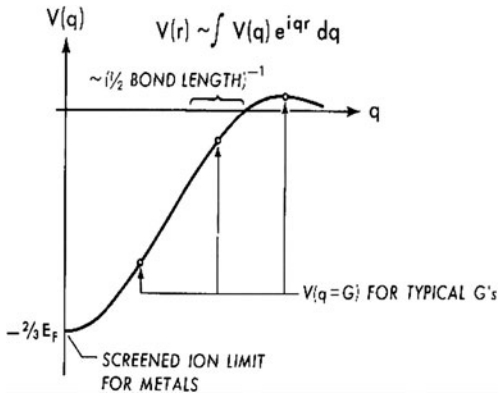



FIG. 3. Schematic drawing of a pseudopotential in reciprocal space.

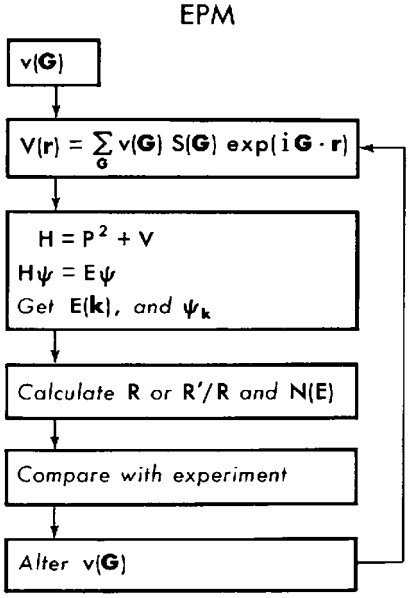



FIG. 4. Block diagram illustrating the empirical pseudopotential method (EPM) approach.

https://doi.org/10.1557/jmr.2011.328 Published online by Cambridge University Press

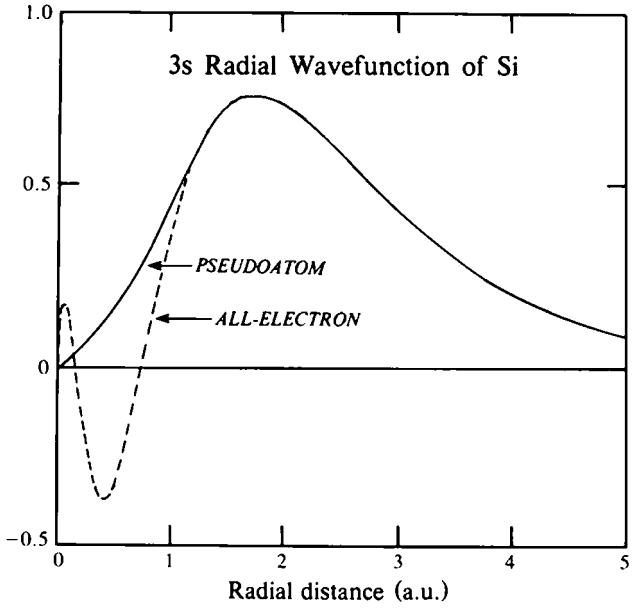



FIG. 5. The construction of an ab initio pseudopotential.

functional theory within the local-density approximation (LDA),[10] it was possible to calculate the total energy of a solid for a specific crystal structure.[11,12] This was first applied to study high-pressure phases of Si and Ge.[13] The energy versus volume $E(V)$ for Si calculated using this method is given in Fig. 6.

The lattice constants, bulk moduli, and transition volumes and pressures are obtained in these studies. Several of the high-pressure phases of Si were predicted using this approach. By inputting the atomic masses, this total energy approach could be used to calculate phonon spectra and electron–phonon interaction parameters. Hence, many properties of solids could be calculated with only the crystal structure and the atomic numbers and masses as input. The use of the supercell concept[14] made it possible to deal with complex structures and multiatom systems. It is interesting to note that once the inner workings of the ab initio and EPM are understood, then semiempirical theories can be developed for calculating specific properties. An example is that, it can be shown that the bulk modulus for group IV, III-V, II-VI diamond and zincblende semiconductors is proportional to the bond length to the −3.5 power. Using relationship and a single ionicity parameter for the III-V's and double that parameter for all the II-VI semiconductors, it is possible to obtain accuracy of less than 2% for these materials.[15,16]

Despite the success of the above approach for calculating ground state properties, because the LDA does not give excited state (quasiparticle states) accurately, usually band gaps are underestimated. Hence unlike the EPM, this ab initio method could not give optical spectra in agreement with experiment. Two major improvements in recent years have been based on many-body theory. The

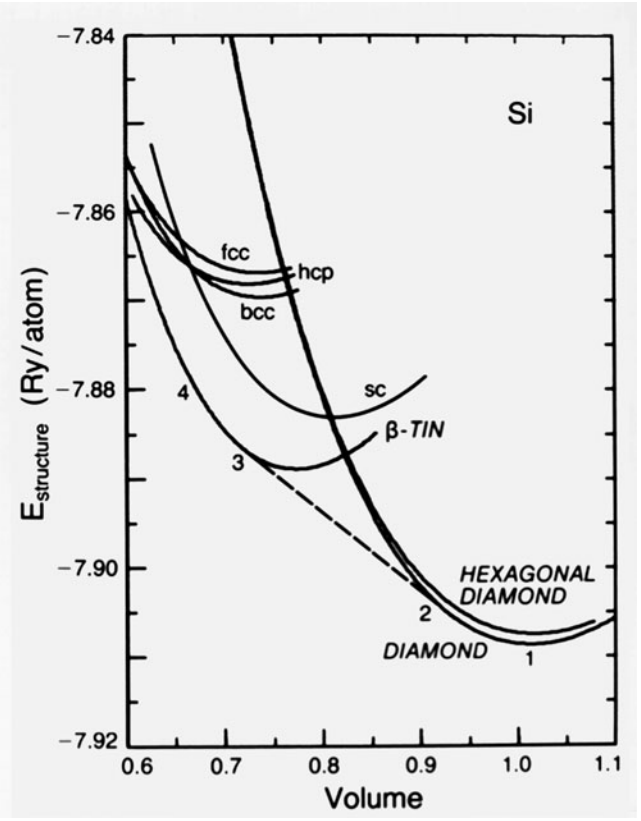



FIG. 6. Calculated total energies as a function of volume for several structures of silicon.

first is called the GW approach[17] which is used to obtain quasiparticle energies, and the second involves the use of the Bethe–Salpeter equation[18] to compute the effects arising from the interaction between an electron and a hole produced in an optical transition. With these modifications, band gaps and optical spectra can be computed from first principles.

## III. PHOTOVOLTAICS AND WAVE FUNCTION ENGINEERING

Silicon has been the prototype material for application in photovoltaic devices. Despite the fact that the absorption spectra of other materials can match the solar spectrum more effectively, the well-developed processing techniques and other properties of Si make it a very desirable material for this application. The purpose of this study is to explore the possibility of improving Si so that a better match with the solar flux of photons can be attained using a modified Si material (see Fig. 7). One way to modify Si is to use alloying or doping; another is to consider another structural phase induced by pressure and stabilized at atmospheric pressure. Here, we consider the latter case and focus on the structural phase called the R8 or Si XII phase. This phase can be made by using pressure on the diamond structure phase to induce a transformation

https://doi.org/10.1557/jmr.2011.328 Published online by Cambridge University Press

to the metallic gray tin phase, and then release the pressure to produce the R8 phase.[19]

The concept and application of "band gap engineering" proposes that a property of a semiconductor is changed to change its band gap. The most popular example is alloying. The EPM was used to show how alloying various semiconductors would change the gaps and hence their optical responses. This concept is illustrated in Fig. 8, where the desired band gap is represented by a red line, and the changes in the semiconductor band gap by changing a parameter, such as alloy concentration, is represented by $x$. A possible problem for photovoltaic applications of this approach is that even if the band gap is optimized, the absorption may not be. For example, for Si, several proposals to change Si from an indirect gap material to a direct gap semiconductor suggest moving the minimum conduction band state usually located near the X point of the Brillouin zone to the center of the zone directly above the valence band state. Although this can be achieved, the matrix element for optical transitions does not change much. Calculations show that the wave function corresponding to the conduction band state "remembers" its form after the artificial movement of the k-point of this state. The top valence band state in Si is p-like and it puts electron density in the covalent bond. The minimum conduction band state puts electronic density (if occupied) in the interstitial region and the resulting dipole matrix element between these states is small.

What is needed for photovoltaics is high optical absorption at the desired frequency, and this requires that attention be given to the wave functions of the states involved in the absorption process. Schematically, in Fig. 8, this motivation is illustrated by changing the variable $x$ to give a peak (indicated by the red arrow) in absorption at the desired frequency. This is what is achieved in the schematic drawing for modified Si in Fig. 7. The results for the calculations for R8 (Si XII) are shown in Fig. 9 along with measured results for Si in the diamond structure ($c$-Si), polycrystalline and amorphous (alpha) Si. This plot clearly shows the increased absorption for R8 near the solar spectrum peak.

Although a very thick sample will absorb equally for all the above cases, it is desirable to have a sample as thin as possible. If we compute the energy absorbed $W$ as a function of the thickness $L$ for a solar intensity $I(E)$ for samples of different absorption coefficients $\alpha(E)$, we have the expression

$$W(L) = \int_0^\infty \left(1 - e^{-\alpha(E)L}\right) I(E)dE \quad .$$

By solving this equation for the Si modifications shown in Fig. 9, we have determined the absorption

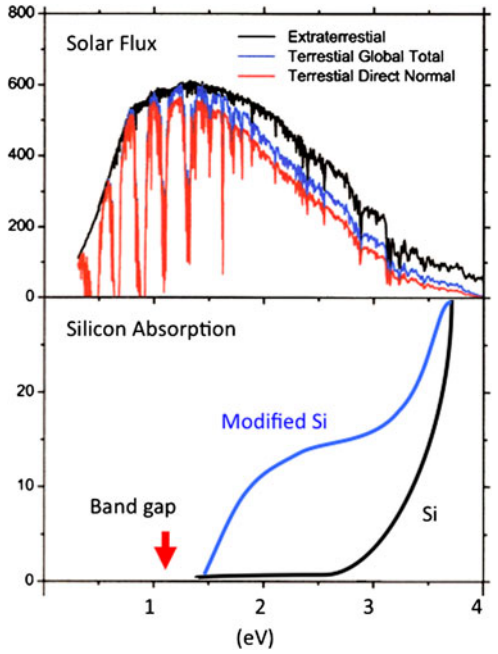



FIG. 7. Schematic drawing of the comparison of the absorption spectrum of silicon and modified silicon with the solar spectrum.

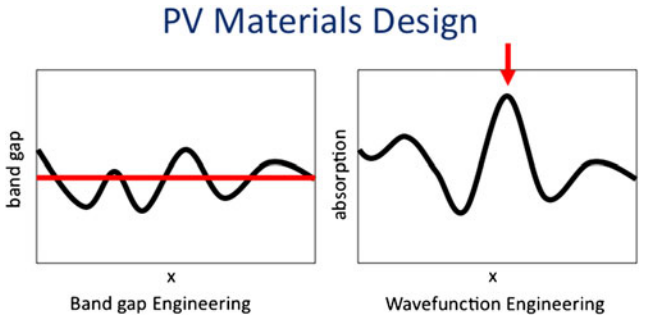



FIG. 8. Schematic drawing illustrating the band gap engineering and wave function engineering approaches for finding suitable photovoltaic materials.

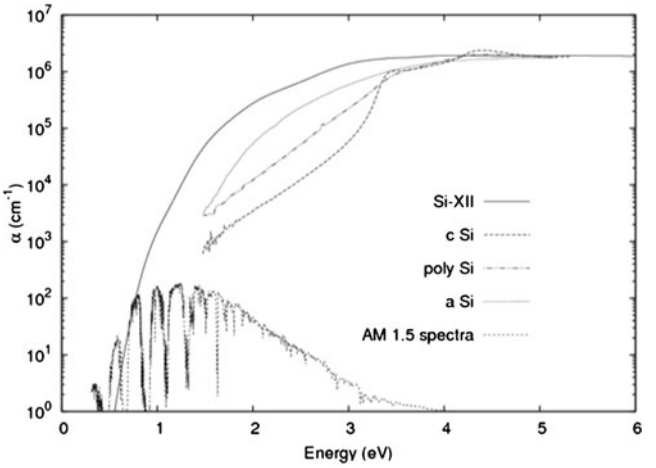



FIG. 9. Comparison of the absorption spectrum of some structural forms of silicon with the solar spectrum.

https://doi.org/10.1557/jmr.2011.328 Published online by Cambridge University Press

percentage as a function of absorber thickness. As shown in Fig. 10, Si XII can be made thin and absorb as much as much thicker samples of Si in the other modifications. Current research on this material, both experimental[20] and theoretical, is very encouraging. However, even if this modification of Si is not the best choice, this direction of research and development may hold promise for creating better voltaics through wave function engineering.

## IV. BORON NITRIDE NANOTUBES

As in the case of the study of the optical properties of semiconductors, the study of boron nitride nanotubes (BNNTs) is another example of how theoretical and experimental research leads to the development of new understandings of nanostructures. Although most studies of nanostructures have focused on carbon materials, novel structures of this kind are not limited to carbon. For BNNTs, one can think of the hexagonal boron nitride (h-BN) sheet as the building block in analogy to graphene for a carbon nanotube (CNT). A rolled up sheet of h-BN is shown in Fig. 11. In fact, many of the interesting properties of h-BN are found in BNNTs, including large electronic band gap, strikingly white color, thermal stability to extreme temperatures in oxidizing environments, and neutron radiation absorption and shielding.

The possible existence of BNNTs was predicted by theory,[21] and they were synthesized[22] soon afterward. The successes related to the prediction of the existence of these systems and some of their properties gave further credibility to the idea that the calculation techniques discussed above for bulk solids can be used for nanoscale objects. Until recently, because of the difficulties associated with producing large quantities of BNNTs, studies of these systems have been limited. Fortunately, new growth techniques[23] are yielding larger quantities and research and applications are increasing.

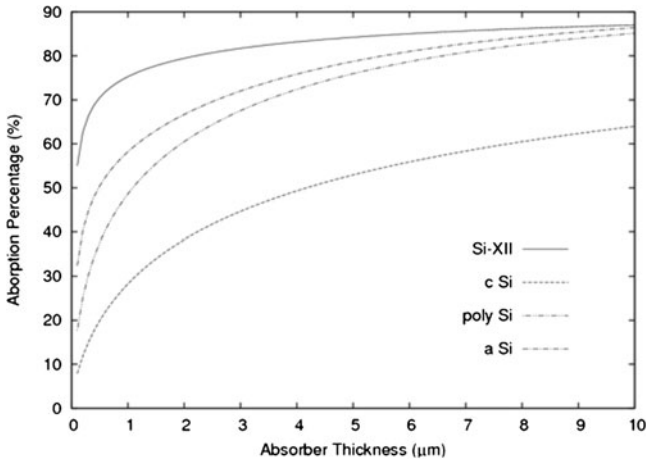



FIG. 10. Absorption percentage of the solar flux versus absorber thickness for some structural forms of silicon.

BNNTs are, relative to their planar parent, more stable than CNTs [see Fig. 12(a)], and when they are produced, it is difficult to destroy them. They can be multiwalled like CNTs. Figure 12(b) shows transmission electron microscope images of various BNNTs with wall number $N$ ranging from 1 to 6. In addition, a so-called "silo" tube is

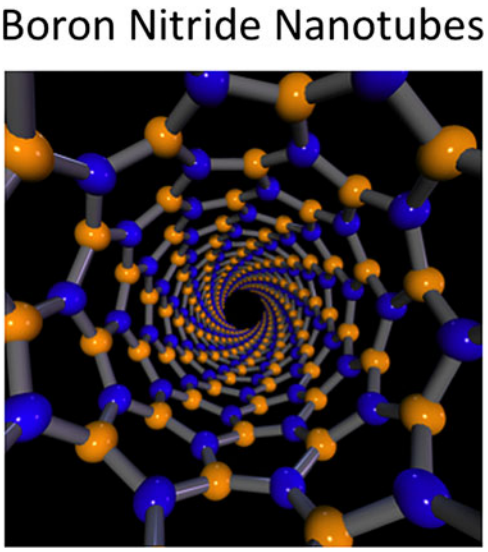



FIG. 11. Ball and stick model of the structure of a boron nitride nanotube (BNNT).

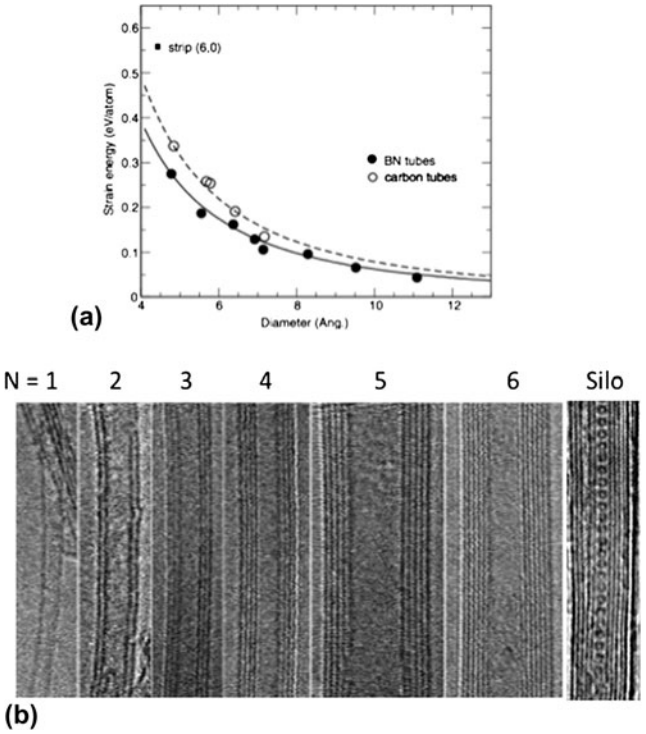



FIG. 12. (a) Calculated strain energy versus radius showing the relative stability of BNNT and carbon nanotube. (b) Electron microscopy of multiwalled BNNTs and a silo BNNT containing C60 molecules.

https://doi.org/10.1557/jmr.2011.328 Published online by Cambridge University Press

shown. This is a multiwalled tube containing C60 molecules. Compared with CNTs, the electronic properties of BNNTs are relatively insensitive to geometrical variations. In fact, the BNNTs in the first six panels of Fig. 12(b) have similar semiconducting electronic structure. This means that the difficult job of separating semiconducting and metallic nanotubes, which is necessary for CNTs, can be avoided. In addition to pseudopotential total energy methods within the LDA and quasiparticle extensions of pseudopotential theory, tight binding models were used to study and predict the structural and electronic properties of BNNTs. The polar nature of the boron nitride bond led to the theoretical prediction that, in contrast to CNTs, BNNTs would, as mentioned above, be semiconductors irrespective of their differing diameters and chiralities.[24] The calculated band gap, in the range of 5 eV, is consistent with optics studies. A plot of the band structure $E(k)$ is shown in Fig. 13(a) using the LDA. Hence, the band gap for this calculation is underestimated. The calculations predict that with doping, either within the tube wall or via functionalization, the electronic properties can be changed considerably. As an example, the electronic structure associated with the lowest conduction band of BNNTs is interesting because if the tube is doped n-type to occupy this state, the electronic charge resides inside the tube, not on it, with a maximum value of the charge density occurring about 2 Å in from the wall of the tube. Hence these n-doped tubes should act like pipes filled with "free" electrons as shown schematically in Fig. 13(b). In addition, BNNTs have been shown[25] to be excellent electron field emission sources, with emission turn-on voltages comparable to those for CNTs. In contrast to CNT field emitters, BNNT field emitters display extremely stable field emission currents.

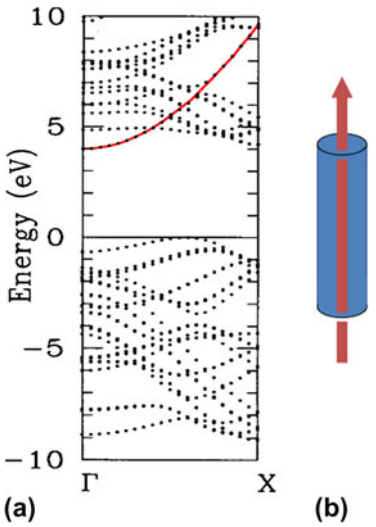



FIG. 13. (a) The electronic band structure of a BNNT. (b) Schematic drawing illustrating the charge density associated with electrons in the lowest conduction band for a doped BNNT.

An interesting theoretical prediction is that the band gaps of BNNTs can be externally tuned.[26] The minimum band gap of BNNTs can be reduced with sufficiently strong electric fields. This "giant Stark effect" is analogous to the conventional Stark effect for atomic orbitals. The mixing of electronic states in BNNTs in transverse electric fields is enhanced because of the field-induced splitting of the electronic bands with states having their electron and hole densities on opposite sides of the BNNT. The reduced screening, because of the insulating behavior, allows a significant difference in the electric potential seen at the two sides of the tube. Hence states that in the absence of a field would be degenerate with similar wave functions at opposite sides of a tube are now split. The effect depends on tube diameter as shown in Fig. 14. There is experimental confirmation for this effect.[27]

Because of their novel properties, the study of BNNTs may provide an opportunity to study novel physical phenomena and applications.[28] Some possibilities are shown in Figs. 15 and 16.

## V. SUPERCONDUCTIVITY IN MODIFIED SEMICONDUCTORS AND INSULATORS

It has been 100 years since the discovery of superconductivity in Hg.[29] The theory explaining this discovery came 46 years later with the seminal work of Bardeen, Cooper, and Schrieffer (BCS),[30] which completely explained the properties of superconductors discovered up to that time. A major early goal was to find superconductors with high transition temperatures. However, the maximum transition temperature for superconductors increased on an average of only 1 °C every 3 years until the late 1980s when superconductivity was discovered in materials based on copper and oxygen.[31] The highest transition temperature observed in systems of this type is around 165 K,[32] and that is the current record.

After the original discovery of superconductivity, many materials were tested. It was quickly found that

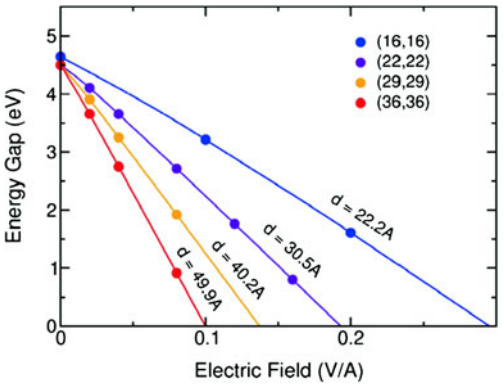



FIG. 14. Calculate dependence of the band gap as a function of the strength of an applied electric field transverse to a BNNT.

https://doi.org/10.1557/jmr.2011.328 Published online by Cambridge University Press

only metals exhibited superconductivity, so having conduction electrons is crucial. Semiconductors and insulators are therefore not expected to exhibit superconducting properties unless they are doped or modified in other ways to make them conduct at low temperatures. In the 1960s, the possibility of superconductivity in degenerately doped semiconductors using model systems[33,34] motivated experimental searches, and within a short time, superconductivity was found in GeTe,[34] SnTe,[34] and $SrTiO_3$.[35] These were all doped low carrier density systems, and the transition temperatures were below 1 K. Since this early work, more low carrier density superconductors have been found.

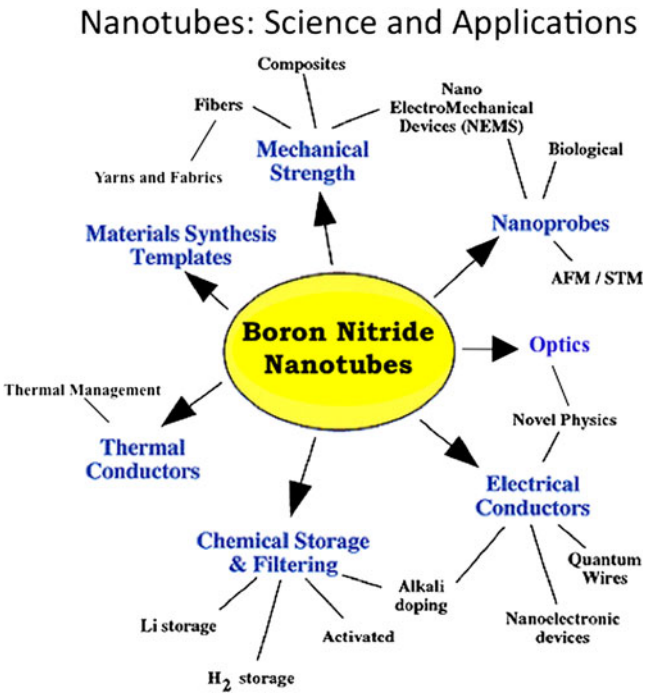



FIG. 15. Chart of applications and properties of BNNTs.

It is useful to separate superconducting materials into two classes 1 and 2 as shown in Fig. 17 to discuss the role that theory has played in explaining and predicting properties and even the existence of new superconductors. Class 1 contains "conventional BCS superconductors" like Al, Sn, Pb, Hg, etc. For these materials there are many experimental tests showing that the BCS theory is applicable. The same can be said for the other members of this class, such as degenerate semiconductors. The BCS theoretical description of their superconducting properties based on electron pairing induced by electron–phonon coupling works extremely well, and it is possible to use the theory to predict new superconductors. In this article, we will restrict ourselves to class 1 materials, since for class 2, as mentioned above, there is no consensus at this time regarding the correct theory to explain their properties. For class 1, it is generally accepted that all experimental data have been explained. In some applications of the theory, such as the calculation of $T_c$, the precision needed has not been achieved in general. However, this shortcoming is usually attributed to our inability to calculate the needed input to the BCS theory, i.e., the normal state properties, with sufficient precision.

What about the highest $T_c$'s? The current upper limit record for class 1 is around 40 K for $MgB_2$. Although this

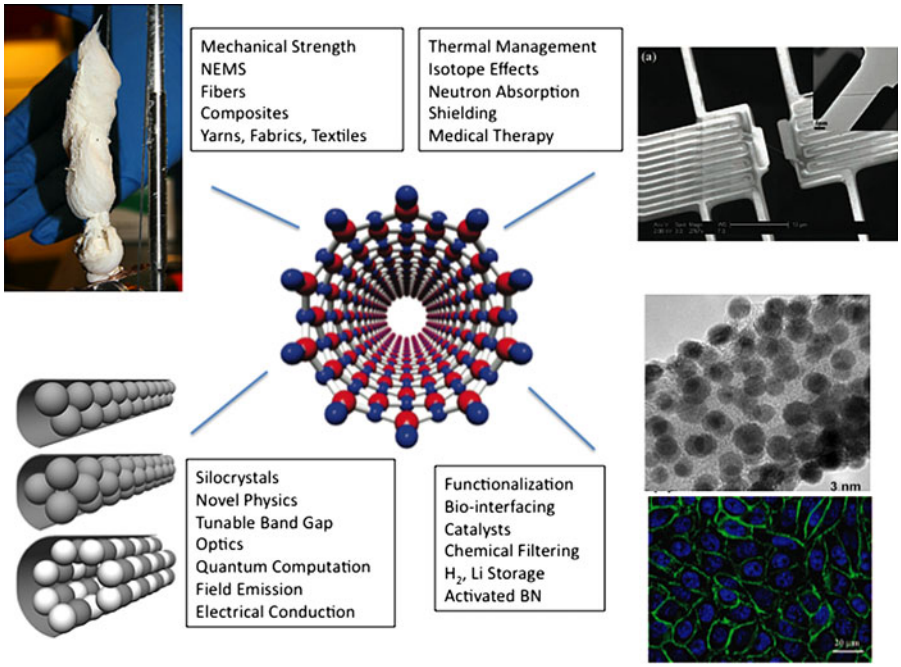



FIG. 16. Examples of applications and properties for functionalized BNNTs.



https://doi.org/10.1557/jmr.2011.328 Published online by Cambridge University Press

is significantly lower than for materials in class 2, it is still difficult to predict whether the next record breaking $T_c$ will be for a material in class 1 or class 2. The advantage of studying this problem for class 1 is that the theory is well established and to a great extent understood for some materials systems, hence possible paths to higher $T_c$ values can be explored. Just after the publications of the BCS theory, the most commonly used expression for calculating $T_c$ was the BCS expression listed in Fig. 18. This formula for $T_c$ is based on "the BCS Model" which assumed a weak coupling pairing interaction $N(0)V$, where $V$ is the net attractive pairing potential and $N(0)$ is the density of states at the Fermi energy. The exponential dependence of $T_c$ on $N(0)$ is the reason for the strong focus on this quantity for increasing $T_c$. The interaction $V$ is composed of an attractive phonon component and the repulsive Coulomb potential. These compete as seen in the following formula for the transition temperature $T_c$ based on the BCS model

$$T_c \sim E(\text{phonon}) \exp[(-1/(\lambda - \mu^*)] \quad .$$

Here, $E$(phonon) represents an average energy of the phonons such as the Debye temperature, and the net interaction in the exponent is the dimensionless phonon pairing interaction $\lambda$ and the modified repulsive electron–electron interaction $\mu^*$. These are the two components of $N(0)V$, i.e., $N(0)V$ can be viewed as $\lambda - \mu^*$. Superconductivity is expected when this difference is positive. The Coulomb interaction is modified (hence the asterisk superscript) because of the difference in energy scales between the two pairing potentials.

McMillan[36] included the effects of renormalization and of stronger coupling when the electron–phonon parameter $\lambda$ became larger. This equation (Fig. 18) can be used for values of $\lambda$ up to about 1.25. The McMillan equation became the $T_c$ equation of choice, and it is still used. However, applications beyond the above limit led to incorrect estimates of the maximum transition temperature. This gave a pessimistic view since the resulting expression for $T_c(\lambda)$ for the McMillan equation saturates. Later, Allen and Dynes[37] (Fig. 18) solved the Eliashberg[38] equations for several model phonon spectra and found that, for large $\lambda$, $T_c$ was proportional to $\lambda^{1/2}$ (Fig. 18) with no saturation.

Modern calculations of $T_c$ are usually done by solving the Eliashberg equations numerically. This approach gives precise estimates when precise normal state properties are used as input. There are model solutions that result in simple formulas (for $\mu = 0$) such as the Kresin–Barbee–Cohen model[39,40] based on a flat phonon spectrum,

$$T_c = 0.25\sqrt{<\omega^2>}\left(e^{2/\lambda} - 1\right)^{-1/2} \quad ,$$

where $<\omega^2>$ is an appropriately averaged square of the phonon frequency. This expression gives the correct $\lambda^{1/2}$ limit at high $\lambda$ and the exponential BCS model solution for small $\lambda$.

Because of these developments, the shift in searching for higher $T_c$ changed from a search for large $N(0)$ materials to looking for large $\lambda$'s. The separation into $N$ and $V$ suggested by the $NV$ parameter is not appropriate for most materials since most systems are not modeled well by the BCS model solution. When considering the shift from looking for large $N(0)$ to large $\lambda$'s, an important caveat to add is that strong electron–phonon interactions often lead to structural instabilities. Hence, when considering large $\lambda$'s, an important caveat is that strong electron–phonon interactions often lead to structural instabilities as described earlier. Therefore, the desired material may not be stable at atmospheric pressure.

As discussed above, successes using ab initio calculations came with the development of the Eliashberg theory and the advances made in calculating normal state properties. To illustrate some of the features of this approach for phonon-mediated pairing, an expression for calculating $\lambda$ is given in Fig. 18 in terms of the Eliashberg spectral function which can be viewed as the product of the electron–phonon coupling times the phonon density of states,

CLASSES OF SUPERCONDUCTORS

[1] BCS: conventional metals, C60, some organics, doped semiconductors, MgB2, ...

---

[2] EXOTIC: copper oxides, heavy fermion metals, some organics, Fe and Ni based materials,...

FIG. 17. Classes of superconductors.

$T_c$ formulas

$$T_c = 1.14\omega_{ph}\exp\left(\frac{-1}{N(0)V}\right) \quad \text{BCS, 1957}$$

$$T_c = \frac{T_D}{1.45}\exp\left(-\frac{1.04(1+\lambda)}{\lambda-\mu^*(1+0.62\lambda)}\right) \quad \text{McMillan, 1968}$$

$$T_c = \frac{\langle\omega\rangle_{\log}}{1.20}\exp\left(-\frac{1.04(1+\lambda)}{\lambda-\mu^*(1+0.62\lambda)}\right) \quad \text{for } \lambda < 1.5$$

$$T_c = 0.183\sqrt{\lambda\langle\omega^2\rangle} \quad \text{for } \lambda > 10,\ \mu^*=0 \quad \text{Allen and Dynes, 1975}$$

$$\lambda \equiv 2\int_0^{\omega_{\max}} \alpha^2 F(\omega)\omega^{-1} d\omega$$

FIG. 18. Formulas for calculating the superconducting transition temperature.

https://doi.org/10.1557/jmr.2011.328 Published online by Cambridge University Press

$$\alpha^2 F(\vec{k}, \vec{k}', \omega) \equiv N(\varepsilon_F) \sum_j \left| g^j_{\vec{k}\vec{k}'} \right|^2 \delta(\omega - \omega_{j\vec{q}}) \quad ,$$

where $N(\varepsilon_F)$ is the density of states per spin at the Fermi level, $g_{kk'}$ is the electron–phonon matrix element, and $\omega_{j\vec{q}}$ is the frequency of the phonon. It is often convenient to solve the Eliashberg equations in the Matsubara representation where

$$\lambda(\vec{k}, \vec{k}', n) \equiv \int_0^\infty d\omega \alpha^2 F(\vec{k}, \vec{k}', \omega) \frac{2\omega}{\omega^2 + (2n\pi T)^2} \quad .$$

Here, the conventional λ is represented by the average

$$\langle \lambda = \lambda(\mathbf{k}, \mathbf{k}', 0) \rangle \quad .$$

The first ab initio calculations for semiconductor-based systems were for high-pressure phases of Si.[41] These calculations dealt with the averaged values for the input to the Eliashberg equations, and the approach used a method that had just been developed for calculating electron–phonon couplings. The application to high-pressure Si was a dramatic example of the power of this approach. Using only the atomic number and atomic mass for Si, the total energies for candidate crystal structures were compared at various pressures. Several new forms of Si were successfully predicted. Two of these, simple (or primitive) hexagonal and hexagonal close-packed Si were studied in detail. The existence of these phases, their stability, lattice constants, mechanical properties, electronic structures, vibrational properties, and electron–phonon coupling were then determined from first-principles calculations. The Coulomb potential μ* could be estimated using the densities of states at the Fermi energy as a scaling parameter. The result was a successful prediction of superconductivity for both phases and an estimate of $T_c$ and its pressure dependence. Considering the limited input and the accurate predictions, it could be said that high-pressure Si became the best-understood superconductor.

As mentioned earlier, the quest for higher superconducting transition temperatures began in 1911, and although our theoretical understanding of superconductivity has advanced considerably and successful predictions of new superconductors have been made for class 1 superconductors, we still do not have a consensus on a well-defined path for increasing $T_c$. Fortunately, for strong electron–phonon coupling, the Allen–Dynes limit, which does not saturate, is more optimistic than the McMillan equation, which saturates as the coupling gets stronger. The search for larger electron–phonon couplings also depends on the development of methods capable of calculating the couplings with high precision. The early approach for high-pressure Si was developed to work with a plane wave basis set,[41] and calculations at many points in reciprocal space were needed to obtain a good estimate of λ. A recent development that has many advantages is based on the use of Wannier functions to evaluate electron–phonon couplings.[42] This real space approach is illustrated schematically in Fig. 19 where an electron in one cell is coupled to an electron in another cell via a vibrating atom in a third cell. A typical calculation using this approach can be equivalent to plane wave calculations that would require millions of points in reciprocal space for convergence. In the area we are considering, semiconductors and insulators, we note that applications[42] have been made to explore superconductivity in doped diamond and SiC.[42–44]

Searching for higher $T_c$ materials has become a search for conditions that will lead to large λ's either via large densities of states or through large electron–phonon pairing potentials. An interesting alternative view[45] is to express λ as a dimensionless ratio of electronic and vibrational spring constants

$$\lambda \sim \frac{N(E_F) < I^2 >}{M < \omega^2 >} \quad ,$$

where $<I^2>$ is the square of the displacement-induced electron scattering matrix element averaged over the Fermi surface, $<\omega^2>$ is an average of the square of the phonon frequencies, and $N(E_F)$ is the electronic density of states at the Fermi energy. For harmonic systems, the $M<\omega^2>$ and λ are roughly independent of $M$. Perhaps a better view is to look at $T_c$ for large coupling where

$$T_c \sim (\lambda < \omega^2 >)^{1/2} \sim \left(\frac{\eta}{M}\right)^{1/2} \quad .$$

This equation implies that what is needed for higher $T_c$'s is stronger electronic spring constants and light masses. This can be extended to explore compounds with

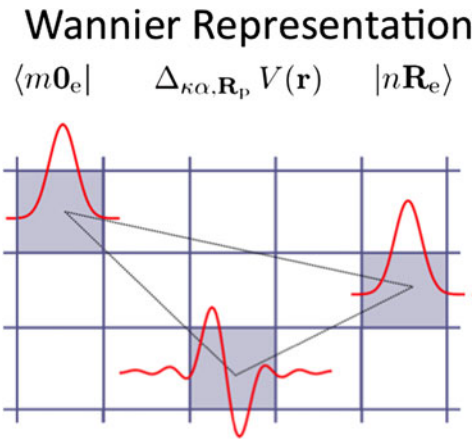



FIG. 19. Schematic drawing showing the Wannier approach for calculating the interaction between two electrons (in rows 1 and 2) via an atomic vibration (in row 3).



https://doi.org/10.1557/jmr.2011.328 Published online by Cambridge University Press

Values of $\eta$

| | $\eta$ (eV/Å$^2$) | $0.183\sqrt{\lambda\langle\omega^2\rangle}$(K) | EXP |
|---|---|---|---|
| C (diamond)* | 54 | 290 | ~ 10 |
| C (graphite)* | 48 | 270 | ? |
| BN* | 36 | 240 | ? |
| Si* | 10 | 82 | ~10 |

*at peak of $\eta$(E)

FIG. 20. The peak values of the electron spring constant and the associated transition temperatures (calculated and measured values) for some materials.

multiple masses in a unit cell, and estimates can be made using information from molecular fragments.[46] We note that strong electronic spring constants are expected for strong bonds such as the covalent bonds in diamond. The challenge in the latter case is getting enough mobile carriers. If one considers the energy dependence of the electronic spring constant, then a possible path to higher $T_c$ is to dope into peaks in the energy-dependent electronic spring constant. A theoretical estimate[45] suggests that very high transition temperatures are possible as shown in Fig. 20. Some success has been reported for experiment,[47] but the $T_c$ level is still not very high.

It is not clear whether class 1 or class 2 type materials are more promising in the search for higher $T_c$'s. The known materials of class 2 have the highest $T_c$'s, but without a descriptive theory, it is difficult to make quantitative predictions. For class 1, it is suggested here that materials with strong bonds and light masses should be studied further. Hence modified semiconductors and insulators appear promising candidates. An encouraging sign is that the transition temperature is expected to increase with the electron–phonon coupling for large values of the coupling. A caveat is that large electron–lattice coupling can result in structural transitions. A possible remedy for this is to choose systems where the integrity of the crystal structure is determined by different bonds than those that couple strongly to the superconducting electrons. This is the case for $MgB_2$.

## ACKNOWLEDGMENTS

This work was supported by the National Science Foundation Grant No. DMR10-1006184 and Director, Office of Science, Basic Energy Sciences, Materials Sciences and Engineering Division of the U.S. Department of Energy under Contract No. DE- AC02-05CH11231.

## REFERENCES

1. M.L. Cohen and J.R. Chelikowsky: *Electronic Structure and Optical Properties of Semiconductors*, 2nd ed. (Springer, Berlin, 1989).
2. M.L. Cohen and T.K. Bergstresser: Band structures and pseudopotential form factors for fourteen semiconductors of the diamond and zincblende structures. *Phys. Rev.* **141**, 789 (1966).
3. M.L. Cohen and V. Heine: The fitting of pseudopotentials to experimental data and their subsequent application, in *Solid State Physics*, Vol. 24, edited by H. Ehrenreich, F. Seitz, and D. Turnbull (Academic Press, New York, 1970), p. 37.
4. E. Fermi: Sullo spostamento per pressione dei termini elevati delle serie spettrali (on the pressure displacement of higher terms in spectral series). *Nuovo Cim.* **11**, 157 (1934).
5. H. Hellman: A new approximation method in the problem of many electrons. *J. Chem. Phys.* **3**, 61 (1935).
6. J.C. Phillips and L. Kleinman: New method for calculating wave functions in crystals and molecules. *Phys. Rev.* **116**, 287 (1959).
7. D.R. Hamann, M. Schluter, and C. Chiang: Norm-conserving pseudopotentials. *Phys. Rev. Lett.* **43**, 1494 (1979).
8. N. Troullier and J. Martins: Efficient pseudopotentials for plane-wave calculations. *Phys. Rev. B* **43**, 1993 (1991).
9. D. Vanderbilt: Optimally smooth norm-conserving pseudopotentials. *Phys. Rev. B* **32**, 8412 (1985).
10. W. Kohn and L.J. Sham: Self-consistent equations including exchange and correlation effects. *Phys. Rev.* **140**, A1133 (1965).
11. J. Ihm, A. Zunger, and M.L. Cohen: Momentum-space formalism for the total energy of solids. *J. Phys. Chem.* **12**, 4409 (1979).
12. M.L. Cohen: Pseudopotentials and total energy calculations. *Phys. Scr. T.* **1**, 5 (1982).
13. M.T. Yin and M.L. Cohen: Microscopic theory of the phase transformation and lattice dynamics of Si. *Phys. Rev. Lett.* **45**, 1004 (1980).
14. M.L. Cohen, M. Schlüter, J.R. Chelikowsky, and S.G. Louie: Self-consistent pseudopotential method for localized configurations: Molecules. *Phys. Rev. B* **12**, 5575 (1975).
15. M.L. Cohen: Calculation of bulk moduli of diamond and zinc-blende solids. *Phys. Rev. B* **32**, 7988 (1985).
16. M.L. Cohen: Theory of bulk moduli of hard solids. Mater. *Sci. Eng., A* **105**(106), 11 (1988); in *Proceedings of 3rd Conference on Science of Hard Materials* (Elsevier, Oxford, 1988), p. 11.
17. M.S. Hybertsen and S.G. Louie: Electron correlation semiconductors and insulators: Band gaps and quasiparticle energies. *Phys. Rev. B* **34**, 5390 (1986).
18. M. Rohlfing and S.G. Louie: Electron-hole excitations and optical spectra from first principles. *Phys. Rev. Lett.* **81**, 2312 (1998).
19. B.D. Malone, J.D. Sau, and M.L. Cohen: Ab initio study of the optical properties of Si-XII. *Phys. Rev. B* **78**, 161202(R) (2008).
20. S. Ruffell, K. Sears, A.P. Knights, J.E. Bradby, and J.S. Williams: Experimental evidence for semiconducting behavior of Si-XII. *Phys. Rev. B* **83**, 075316 (2011).
21. A. Rubio, J. Corkill, and M.L. Cohen: Theory of graphitic boron nitride nanotubes. *Phys. Rev. B* **49**, 5081 (1994).
22. N.G. Chopra, R.J. Luyken, K. Cherrey, V.H. Crespi, M.L. Cohen, S.G. Louie, and A. Zettl: Boron nitride nanotubes. *Science* **269**, 966 (1995).
23. M.W. Smith, K.C. Jordan, C. Park, J-W. Kim, P.T. Lillehei, R. Crooks, and J.S. Harrison: Very long single- and few-walled boron nitride nanotubes via the pressurized vapor/condenser method. *Nanotechnology* **20**, 505604 (2009).
24. X. Blasé, A. Rubio, S.G. Louie, and M.L. Cohen: Stability and band gap constancy of boron nitride nanotubes. *Europhys. Lett.* **28**, 335 (1994).
25. J. Cumings and A. Zettl: Field emission and current-voltage properties. *Solid State Commun.* **129**, 661 (2004).
26. K.H. Khoo, M.S.C. Mazzoni, and S.G. Louie: Tuning the electronic properties of boron nitride nanotubes with transverse electric fields: A giant dc Stark effect. *Phys. Rev. B* **69**, 201401 (2004).

https://doi.org/10.1557/jmr.2011.328 Published online by Cambridge University Press

27. M. Ishigami, J.D. Sau, S. Aloni, M.L. Cohen, and A. Zettl: Observation of the giant Stark effect in boron-nitride nanotubes. *Phys. Rev. Lett.* **94**, 056804 (2005).
28. M.L. Cohen and A. Zettl: The physics of boron nitride nanotubes. *Phys. Today* **63**, 34 (2010).
29. H.K. Onnes: The superconductivity of mercury. *Comm. Phys. Lab. Univ. Leiden*, 120b, 122b, 124c (1911).
30. J. Bardeen, L.N. Cooper, and J.R. Schrieffer: Theory of superconductivity. *Phys. Rev.* **108**, 1175 (1957).
31. J.G. Bednorz and K.A. Muller: Possible high Tc superconductivity in Ba-La-Cu-O system. *Z. Phys. B* **64**, 189 (1986).
32. L. Gao, Y. Xue, F. Chen, Z. Xiong, R.L. Meng, D. Ramirez, and C.W. Chu: Superconductivity up to 164 K in $HgBa_2Ca_{m-1}Cu_mO_{2m+2+\delta}$ (m=a, 2, and 3) under quasihydrostatic pressures. *Phys. Rev. B* **50**, 4260 (1994).
33. M.L. Cohen: Superconductivity in many-valley semiconductors and in semimetals. *Phys. Rev.* **134**, A511 (1964).
34. M.L. Cohen: Superconductivity in low-carrier-density systems: Degenerate semiconductors, in *Superconductivity*, edited by R.D. Parks (Marcel Dekker, Inc., New York, 1969), p. 615.
35. J.F. Schooley, W.R. Hosler, and M.L. Cohen: Superconductivity in semiconducting $SrTiO_3$. *Phys. Rev. Lett.* **12**, 474 (1964).
36. W.L. McMillan: Transition temperature of strong-coupled superconductors. *Phys. Rev.* **167**, 331 (1968).
37. P.B. Allen and R.C. Dynes: Transition temperature of strong-coupled superconductors reanalyzed. *Phys. Rev. B* **12**, 905 (1975).
38. G.M. Eliashberg: Interactions between electrons and lattice vibrations in a superconductor. *Sov. Phys. JETP* **11**, 696 (1960).
39. V.Z. Kresin: On the critical temperature for any strength of the electron-phonon coupling. *Phys. Lett. A* **122**, 434 (1987).
40. L.C. Bourne, A. Zettl, T.W. Barbee, III, and M.L. Cohen: Complete absence of isotope effect in $YBa_2Cu_xO_7$: Consequences for phonon-mediated superconductivity. *Phys. Rev. B* **36**, 3990 (1987).
41. K.J. Chang, M.M. Dacorogna, M.L. Cohen, J.M. Mignot, G. Chouteau, and G. Martinez: Superconductivity in high-pressure metallic phases of Si. *Phys. Rev. Lett.* **54**, 2375 (1985).
42. F. Giustino, M.L. Cohen, and S.G. Louie: Electron-phonon interaction using Wannier functions. *Phys. Rev. B* **76**, 165108 (2007).
43. J.E. Moussa and M.L. Cohen: Constraints on Tc for superconductivity in heavily boron-doped diamond. *Phys. Rev. B* **77**, 064518 (2008).
44. J. Noffsinger, F. Giustino, S.G. Louie, and M.L. Cohen: Origin of superconductivity in boron-doped silicon carbide from first principles. *Phys. Rev. B* **79**, 104511 (2009).
45. J.E. Moussa and M.L. Cohen: Two bounds on the maximum phonon-mediated superconducting transition temperature. *Phys. Rev. B* **74**, 094520 (2006).
46. J.E. Moussa and M.L. Cohen: Using molecular fragments to estimate electron-phonon coupling and possible superconductivity in covalent materials. *Phys. Rev. B* **78**, 064502 (2008).
47. E.A. Ekimov, V.A. Sidorov, E.D. Bauer, N.N. Mel'nik, N.J. Curro, J.D. Thompson, and S.M. Stishov: Superconductivity in diamond. *Nature* **428**, 542 (2004).


https://doi.org/10.1557/jmr.2011.328 Published online by Cambridge University Press